ThesisTitle

by

Daniel C. Cole

Other Degrees

A thesis submitted to the

Faculty of the Graduate School of the

University of Colorado in partial fulfillment

of the requirements for the degree of

Doctor of Philosophy

Physics Physics

2018

This thesis entitled:
ThesisTitle
written by Daniel C. Cole
has been approved for the Physics Physics

_____

Reader1

_____

Reader2

Date _____

The final copy of this thesis has been examined by the signatories, and we find that both the
content and the form meet acceptable presentation standards of scholarly work in the above
mentioned discipline.

Cole, Daniel C. (Ph.D., Physics)

ThesisTitle

Thesis directed by Dr. Scott A. Diddams

Optical frequency combs have revolutionized precision metrology by enabling measurements of optical frequencies, with implications both for fundamental scientific questions and for applications such as fast, broadband spectroscopy. In this thesis, I describe the development of comb generation platforms with smaller footprints and higher repetition rates, with the ultimate goal of bringing frequency combs to new applications in a chip-integrated package. I present two new types of frequency combs: electro-optic modulation (EOM) combs and Kerr-microresonator-based frequency combs (microcombs). First I describe the EOM comb scheme and, in particular, techniques for mitigating noise in the comb generation process, and I present the results of a proof-of-principle metrology experiment and some possible applications. Then I discuss developments in microcomb technology. I present novel soliton crystal states, which have highly structured fingerprint optical spectra that correspond to ordered pulse trains exhibiting crystallographic defects. These pulse trains arise through interaction of the solitons with avoided mode-crossings in the resonator spectrum. Next, I describe the direct and deterministic generation of single microresonator solitons using a phase-modulated pump laser. This technique removes the dependence on initial conditions that was formerly a universal feature of these experiments, presenting a solution to a significant technical barrier to the practical application of microcombs. I also discuss generation of Kerr combs in the Fabry-Perot (FP) geometry. I introduce a nonlinear partial differential equation describing dynamics in an FP cavity and discuss the differences between the FP geometry and the ring cavity, which is the geometry used in previous Kerr-comb experiments. Finally, I discuss a technique for reducing the repetition rate of a high-repetition-rate frequency comb, which will be a necessary post-processing step for some applications. I conclude with a discussion of avenues for future research, including the chip-integration of Fabry-Perot Kerr resonators and the use of band-engineered photonic crystal cavities to further simplify soliton generation.

Acknowledgements

The work in this thesis would not have been possible...

- Acknowledgement line 1

- Acknowledgement line 2

Contents

Figures

Chapter 1

Pulse Picking

This chapter presents a discussion of a technique for repetition-rate reduction of optical pulse trains. While high pulse train repetition rates are appealing for some applications, they are not always appropriate. For example, spectral resolution in spectroscopy applications is sacrificed in a comb with a large mode spacing, and a high repetition rate makes nonlinear optics less efficient at a given average power. This can present a barrier to the generation of octave-spanning spectra for $f - 2f$ self-referencing (see Sec. **??**). On the other hand, in general the size of the comb package sets the scale for the round-trip time, meaning that low-SWAP combs tend to have inherently high repetition rates. Therefore, to increase the flexibility of low-SWAP and high-repetition-rate comb systems in applications, a method for reducing the repetition rate of a pulse train will be useful.

Here I present an investigation of a method for pulse train repetition-rate reduction, or down-sampling, in which an electro-optic gate realized by an RF-driven Mach-Zehnder interferometer periodically transmits an incoming pulse at a frequency lower than the input repetition rate. The basic principle is illustrated in Fig. 1.1. Downsampling via pulse gating, also referred to as 'pulse picking' in the literature, has been used extensively in the context of high-field, phase-sensitive ultra-fast optics for the generation of energetic, carrier-envelope-phase-stabilized ultrashort pulses [1, 2]. In this application, a comb with initial repetition rate in the ∼100 MHz range that has already been self-referenced and stabilized is pulse-picked to a repetition rate on the order of 1-100 kHz. Concerns in this application center around control and preservation of the carrier-envelope phase in the

pulse-picking and amplification process [3, 4]. In contrast, the focus here is on downsampling within the context of optical metrology with frequency combs, and we are concerned with downsampling's effect on the optical phase noise, the pulse-to-pulse energy fluctuations, and the carrier-envelope offset frequency of the comb. In particular, it is important that the downsampled pulse train is suitable for $f - 2f$ self-referencing.

Sec. 1.1 presents a proof-of-principle experiment in which a 250 MHz pulse train is downsampled to 25 MHz, and then spectrally broadened and self-referenced. A mathematical model of downsampling is presented in Sec. 1.2, and this model informs the discussion of downsampling's effect on the pulse train's noise properties presented in Sec. 1.3 and Sec. 1.4. In Sec. 1.5 I discuss some practical considerations in applications of the technique, including the effect of imperfections in the gating process such as incomplete extinction of rejected pulses.
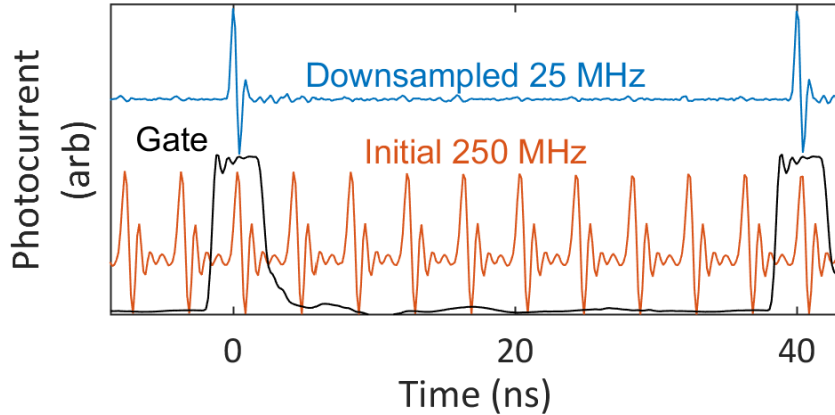

Figure 1.1: **An illustration of pulse-train repetition-rate downsampling.** Orange: A photodetected 250 MHz pulse train. Blue: A photodetected 25 MHz pulse train obtained by downsampling the 250 MHz pulse train by a factor of $N = 10$. Black: Oscilloscope trace showing the voltage sent to the RF port of a Mach-Zehnder intensity modulator to selectively transmit a subset of the incoming pulses. With the intensity modulator biased for zero transmission, the voltage trace is indicative of the transmission.

1.1   Proof-of-Concept Experiment

Here I present a proof-of-concept experiment in which a 250 MHz comb is downsampled and self-referenced. The setup for and results of this experiment are summarized in Fig. 1.2. Our pulse

gating scheme, shown in Fig. 1.2a, employs a Mach-Zehnder (MZ) electro-optic intensity modulator driven by 25 MHz rectangular electronic gating pulses with 80 ps transitions and 3.5 ns duration. The electronic pulse generator and the repetition rate of the input 250 MHz comb are both referenced to a hydrogen maser to maintain synchronization. The DC bias of the intensity modulator is set for maximum extinction outside the electronic gate, whose amplitude is approximately matched to V_π of the EOM. This downsampling scheme results in a stable 25 MHz optical pulse train with >12 dB contrast (Fig. 1.1). This contrast is adequate for this experiment, but could be improved by cascading modulators with higher extinction ratios. The average power of the 250 MHz pulse train is reduced from 30 mW to 400 μW by the pulse gating process and the insertion loss of the optical components. The pulse train is amplified to 35 mW by use of a normal-dispersion erbium-doped fiber amplifier, which provides some spectral broadening and temporal pulse compression [**Fermann2000**]. An octave-spanning supercontinuum is obtained by launching the amplified, <100 fs, ~1 nJ pulses into 20 cm of highly nonlinear fiber (HNLF) [5]; the resulting spectrum is shown in Fig. 1.2b. For comparison, we also present the supercontinuum generated by the 250 MHz comb with the EOM set for constant maximum transmission under otherwise identical conditions. The 250 MHz comb is amplified by the same EDFA to an average power of 85 mW, corresponding to 340 pJ pulse energy, before it enters the HNLF.

To detect f_0, the octave-spanning supercontinuum shown in Fig. 1.2b is sent into a free-space $f - 2f$ interferometer consisting of a half-wave plate and a periodically poled lithium niobate (PPLN) crystal quasi-phase-matched for second-harmonic generation at 1980 nm. The generated 990 nm light is shown in 1.2b. A 10 nm band-pass filter at 990 nm selects this second harmonic and the co-linear supercontinuum at 990 nm, which are then photodetected to observe f_0 with 30 dB signal-to-noise ratio, shown in Fig. 1.2c. Fig. 1.2d shows a 2000 s record of f_0 for the downsampled comb.
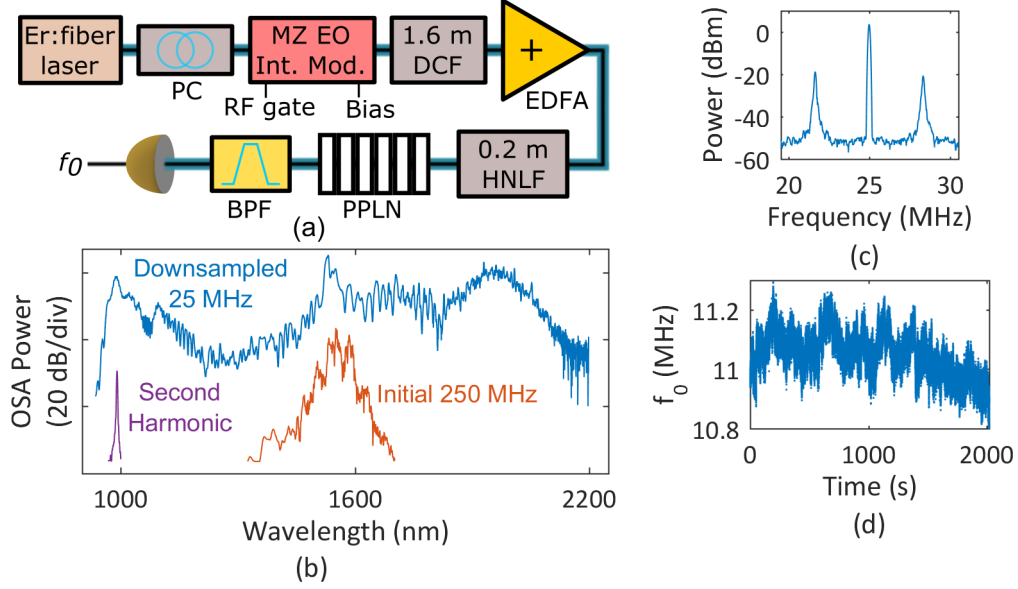
Figure 1.2: **Demonstration of downsampling for f_0 detection.** (a) Schematic depiction of the steup for downsampling a 250 MHz Er:fiber comb and detecting the offset frequency of the resulting 25 MHz pulse train. PC—polarization controller. DCF—dispersion-compensating fiber. EDFA—erbium-doped fiber amplifier. HNLF—highly nonlinear fiber. PPLN—periodically-poled lithium niobate. BPF—(optical) band-pass filter. (b) Octave-spanning supercontinuum generated by downsampling (top, blue), second harmonic generated for f0 detection (purple), and for comparison the supercontinuum generated by the same apparatus without downsampling (orange). (c) Detected repetition rate and f_0 beat at 100 kHz RBW; signal-to-noise ratio of f_0 is 30 dB. e) Counted frequency of the detected free-running offset beat. Data is taken for $\sim$2000 s at 10 ms gate time. The offset frequency of the 250 MHz commercial comb was adjusted between measurements shown in Figs. 1.2c and 1.2d to simplify electronic processing.

1.2   Mathematical model for downsampling

While Fig. 1.2 presents an absolute frequency measurement of f_0 enabled by downsampling, it does not demonstrate the deterministic connection between the input and downsampled combs that is essential for applications. To understand this relationship, I present first a simple model of downsampling, and then experimental tests of its conclusions.

The downsampled pulse train's electric field is modeled as the product of the incoming comb's field and a time-varying amplitude modulation. For an incoming optical frequency comb with repetition rate f_{rep}, complex single-pulse field $A(t)$ that is localized near $t = 0$, and pulse-to-pulse carrier-envelope phase shift ϕ, pulse gating by a train of rectangular pulses of length t_g and arrival

rate f_g yields a downsampled comb with field

$$a(t) = \left[\Sigma_n A(t - n/f_{rep})e^{in\phi}\right] \times \left[\Sigma_m \text{Rect}\left((t - m/f_g)/t_g\right)\right] \tag{1.1}$$

where $\text{Rect}(x)$ is the rectangle function, taking the value 1 for $-1/2 \leq x \leq 1/2$ and 0 elsewhere. Indices n and m count the pulse number of the incoming pulse train and the electronic gate respectively. The optical spectrum of the downsampled pulse train $a(t)$, calculated via the convolution theorem for the Fourier transform, is:

$$\mathcal{F}\{a\}(f) \sim 4\pi f_{rep}\Sigma_{nm}\frac{1}{m}\mathcal{F}\{A\}(f_0 + nf_{rep}) \times \sin(\pi m t_g f_g)\delta(f - f_0 - nf_{rep} - mf_g) \tag{1.2}$$

where $f_0 = f_{rep}\cdot\phi/2\pi$ is the carrier-envelope offset frequency of the incoming comb and δ is the Dirac delta function. The downsampled pulse train has spectral content at optical modes $f_0 + nf_{rep}$, as well as at intensity modulation sidebands whose frequency offsets mf_g are harmonics of the gating frequency. To avoid the generation of unwanted modulations, pulse gating at an integer sub-harmonic of the incoming repetition rate, $f_g = f_{rep}/N$, is essential. In this case superposition of the intensity modulation components created by pulse gating results in a downsampled frequency comb with a single mode spacing. Moreover, this model predicts that the offset frequency is preserved up to a reduction modulo the comb's new repetition rate.

Notably, for pulse gating at a sub-harmonic of the input comb's repetition rate, timing jitter of the electronic gate that is less than its duration does not contribute to noise on the downsampled comb. By modeling jitter as gate-to-gate arrival-time delays Δt_m, it can be shown that the down-sampled comb's amplitude $a(t)$ and spectrum $F\{a\}(f)$ do not deviate from Eqn. 1.1 provided that: (1) The jitter is a sufficiently small $|\Delta t_m| < t_g/2$, i.e., that the optical and electronic pulses are always substantially overlapped, and (2) That the optical pulses are substantially shorter than the electrical pulses, which is true for most systems. Thus, in general we expect that the carrier-envelope offset frequency of the incoming comb is preserved by downsampling even with jitter on the gate signal.

1.3 Experimental investigation of the effect of downsampling on the pulse train's noise properties

We supplement the mathematical model presented above with an experimental investigation of the effects of downsampling on the noise properties of the pulse train. First we consider the effects of technical limitations to ideal downsampling, and then we discuss fundamental effects associated with aliasing of high-Fourier-frequency optical noise and shot noise.

We measure the phase-noise spectrum of the downsampled comb's repetition rate at different points in our apparatus, as shown in Fig. 1.3a. We also plot the phase noise of the 250 MHz comb, which has been shifted by $-10\log_{10}(N^2) = -20$ dB to facilitate comparison [6], and the phase noise of the electronic gate. The downsampled frequency comb's phase-noise spectrum matches that of the 250 MHz comb except for a small increase at $\sim$3 kHz, likely corresponding to the corner in the gate generator's phase noise at the same frequency. The phase noise of the high- and low-frequency ends of the supercontinuum similarly matches the 250 MHz comb below 1 kHz. The higher phase noise in the supercontinuum beyond 1 kHz is above the measurement system's noise floor (including shot noise), despite the reduced optical power available after spectral filtering. This higher noise is likely due to noise generation processes in the HNLF, such as the conversion of amplitude fluctuations on input pulses to timing jitter in the supercontinuum [7].

The timing jitter of our gating pulse train is between 5 ps (obtained by integrating the phase noise plotted in Fig. 1.3 to 100 kHz) and 10 ps (extrapolating constant phase noise to the 12.5 MHz Nyquist frequency and integrating). These jitter values are small relative to the 4 ns repetition period of the incoming optical pulse train. As the repetition rate of the incoming optical pulse train increases to >10 GHz, the gate duration must correspondingly decrease for single-pulse gating, and timing jitter on the gate may become a significant fraction of the gate duration. To explore the effects of timing jitter larger than our pulse generator's inherent 5 to 10 ps, we impose excess jitter on the gating signal. We modulate the relative timing between the gating signal and the incoming optical pulse train at a frequency of 5 MHz with an amplitude of 250 ps. The effect of this jitter is
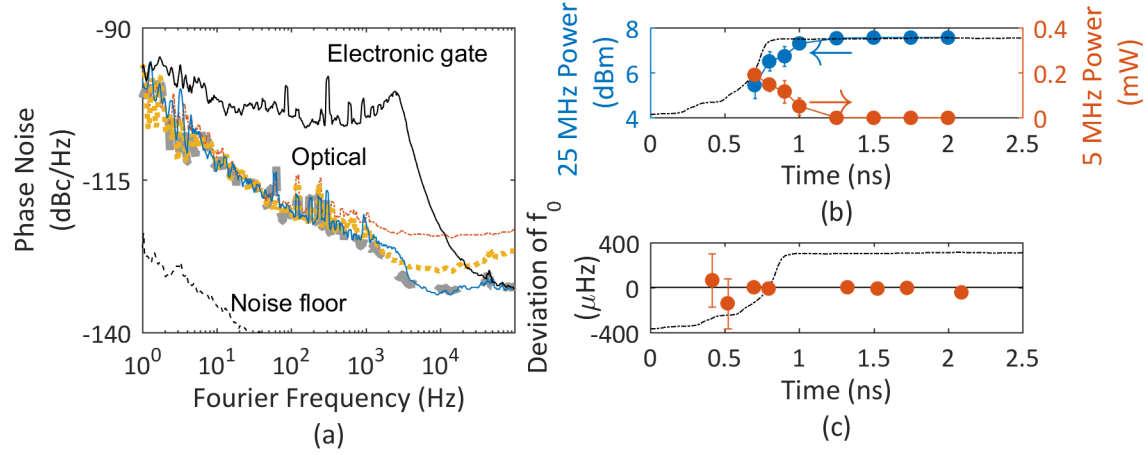
Figure 1.3: **Experimental investigation of noise introduced by downsampling.** (a) Measured repetition-rate phase noise of spectral components of the supercontinuum, selected by a 990±5 nm band-pass filter (dot-dashed orange), 1650 nm long pass filter (dotted yellow), and the entire downsampled 25 MHz frequency comb measured immediately before the EDFA (solid blue), the 250 MHz comb (large-dashed gray, shifted by $20 \log(1/10) = -20$ dB). Also shown is the phase noise of the electronic gate generator (top, solid black). (b) Amplitude of the downsampled pulse-train modulation due to 250 ps jitter at 5 MHz rate. The position of a data point on the x-axis indicates its mean position within the gate, shown in dashed black. Measurement uncertainties arise due to a latency between the optical trigger and the start of the electronic gating signal which varies on the order of 50 ps. (c) Deviation of the carrier-envelope offset frequency of the downsampled comb from the 250 MHz comb's offset frequency as a function of the alignment of optical pulses within the gate.

manifest in the microwave power of the gated comb as 5 MHz intensity-modulation sidebands whose amplitude depends on the position of the optical pulses within the gate, as shown in Fig. 1.3b. Pulses with a mean position within 250 ps of the gate edge are substantially modulated by the 5 MHz gate-delay signal. This agrees with the prediction of a sharp threshold on the acceptable level of timing jitter on the gate.

It is essential to establish that the comb's carrier-envelope offset frequency is preserved in the downsampling process. To do this, we perform a frequency comparison of the 25 MHz downsampled comb and a separate output of the 250 MHz comb. This 250 MHz output is intensity modulated so that a measurement of the nonzero optical heterodyne beat frequency between an intensity modulation sideband and a pulse-gating sideband of the downsampled comb reveals the relative frequency offset of the two combs. Figure 1.3c shows the null frequency shift between the 25 MHz and 250 MHz combs, which we have characterized for different alignments of the optical pulse within the

gate. At the level of several microhertz, better than 10^{-18} relative to the 200 THz optical carrier frequency, we observe no frequency shift between the 250 MHz comb and the downsampled 25 MHz comb when the gate is properly aligned. This confirms the utility of downsampling for measurement of a high-repetition-rate comb's offset frequency for subsequent use of the comb in, for example, a spectroscopy experiment requiring high power per comb mode and high frequency precision.

1.4   Effects of ideal downsampling on a pulse train's noise properties

In addition to the conversion of electronic technical noise to optical noise on the downsampled pulse train, there exists a further mechanism by which downsampling can change the measured amplitude noise properties of the pulse train. Even ideal downsampling, free of electronic noise, leads to an increase in the measured power spectral density (PSD) of optical pulse energy fluctuations (PEF) when technical pulse energy noise is present. This is due to aliasing of components of the PSD of pulse energy fluctuations at frequencies above the Nyquist frequency of the original pulse train, $f_{rep}/2$, when the Nyquist frequency is reduced to $f_{rep}/2N$ by downsampling. Assuming random fluctuations from pulse to pulse, downsampling does not change the RMS fractional pulse energy fluctuation σ_{PEF}, whose square is equal to the frequency integral of the PSD of pulse energy fluctuations $S_{PEF}(f)$:

$$\sigma_{PEF}^2 = \int_0^{f_{rep}/2} df\, S_{PEF}(f). \tag{1.3}$$

—

Because the Nyquist frequency defines the upper limit for integration of S_{PEF}, in order for σ_{PEF} to be preserved $S_{PEF}(f)$ must increase when the Nyquist frequency is reduced by downsampling. For example, in the simple case of white technical noise on the pulse energies with density S_o, we have

$$\sigma_{PEF}^2 = \int_0^{f_{rep}/2} df\, S_o = \int_0^{f_{rep}/2N} df\, S^{'} \tag{1.4}$$

which shows that downsampling must increase the measured PSD of white technical noise from

S_o to $S' = NS_o$, assuming there are no spectral correlations. However, this simple multiplicative increase is restricted to the case of white technical noise. In general, the PSD of pulse energy fluctuations of the new pulse train is determined from the original PSD through the usual method of modeling aliasing of a signal: a new Fourier frequency for each component of the original PSD is obtained by reducing the original Fourier frequency by a multiple of $-f_{rep}/N$ so that it lies between $-f_{rep}/2N$ and $f_{rep}/2N$ and taking its absolute value. The new PSD is then determined by taking the quadrature sum of the PSD components at the same aliased Fourier frequency. This phenomenon is derived mathematically and demonstrated experimentally in Ref. [3], where the analysis of carrier-envelope phase noise applies equally well to pulse energy fluctuations.

In contrast with the increase in the PSD of pulse energy fluctuations arising from coincidence of the optical pulse with the edge of the electrical gate, which increases σ_{PEF}, the aliasing mechanism described above preserves σ_{PEF}. An important consequence of this is that while technical noise can lead to supercontinuum decoherence in external nonlinear spectral broadening, aliasing does not, because it is σ_{PEF} which determines the degree of supercontinuum decoherence. Thus the aliasing mechanism impedes $f - 2f$ self-referencing only by reducing the available signal-to-noise ratio of an f_0 signal in a straightforward linear fashion.

In practice, the relevance of the aliasing of the PSD of pulse energy fluctuations is determined by the presence of technical noise on the pulse energies at high Fourier frequency $f > f_{rep}/2N$. For sufficiently small downsampling factors (e.g. $f_{rep}/2N \leq\sim 50MHz$) and depending on the comb source, it is possible that the only source of intensity noise at frequencies above $f_{rep}/2N$ is shot noise. Shot noise results in a maximal (shot-noise-limited) signal-to-noise ratio (SNR) of an optical heterodyne beat with a local oscillator laser which is reduced by N^2 (in electrical power units) as the average power of the pulse train is reduced by downsampling by a factor of N. In contrast, in the case of detection of a carrier-envelope-offset beat with fixed optical detection bandwidth, the shot-noise-limited SNR is preserved in downsampling. One way to understand these results is to model the shot noise at a given Fourier frequency as the incoherent sum of optical heterodyne beats between each optical comb mode and the uncorrelated vacuum fluctuations at the appropriate optical frequency

[**Bachor1990**, **Quinlan2013**], and to take into account the fact that during downsampling the optical power of each comb mode is reduced by N^2, with the first factor of N coming from reduction of the total optical power and the second factor of N due to the increase in the spectral density of comb modes.

We experimentally investigate the impact of downsampling on the PSD of pulse energy fluctuations by measuring noise on three photodetected optical signals: a shot-noise-limited telecom-band CW laser, a 10 GHz pulse train generated by passing this laser through cascaded optical phase and intensity modulators (see Chapter **??**, [8]) and then a low-noise EDFA, and this pulse train after downsampling by a factor of four to 2.5 GHz repetition rate with no additional amplification after downsampling. Shown in Figure 1.4 are curves for each signal of the fluctuations $\sqrt{S_I(f = 50\,\mathrm{MHz})}$ in the detected photocurrent at a Fourier frequency of 50 MHz versus the total time-averaged detected photocurrent $\langle I \rangle$ from the optical signal. To measure the scaling of noise with optical power, these curves are generated by beginning with an optical signal which yields more than 800 μA of detected photocurrent and attenuating this signal before photodetection. The data indicate that both the pulse-generation process and the downsampling process contribute some amount of technical noise at 50 MHz Fourier frequency to the photocurrent, because the measured curves are well-modeled by a quadrature sum of a shot-noise contribution and a technical noise contribution. The contributions of these two types of noise can be determined because they scale differently with the photodetected power: shot noise obeys the relationship $\sqrt{S_I(f = 50\,\mathrm{MHz})} = \sqrt{2e\,\langle I \rangle}$, $\langle I \rangle$ denoting the time-averaged photocurrent, while the technical-noise contribution arises from fluctuations in the expected photocurrent $I(t)$ and scales linearly with the detected photocurrent. We observe that downsampling by a factor of four leads to a multiplication of the amplitude of the technical noise by a factor of ~1.7 on the optical signal relative to the carrier, which due to finite noise bandwidth is somewhat less than the factor of two (four, in electrical power units) that would be expected for ideal downsampling by a factor of four in the presence of white technical noise. These results further demonstrate that, properly implemented, downsampling does not magnify noise on the pulse train to a degree that is prohibitive for applications.
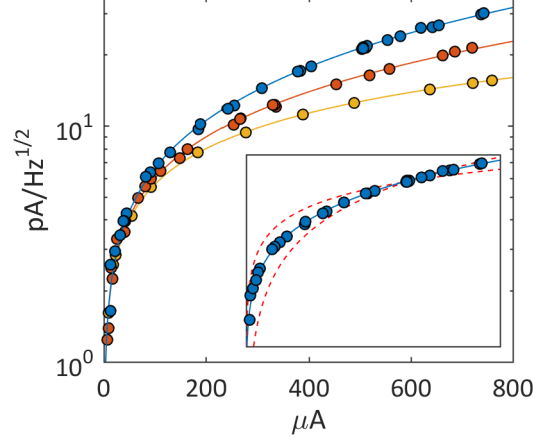
Figure 1.4: **Effect of downsampling on photocurrent fluctuations.** Fluctuations at 50 MHz Fourier frequency in the detected photocurrent as a function of the time-averaged photocurrent in three cases: CW laser at the shot-noise limit (lowest, yellow), 10 GHz pulse train (middle, red), and 2.5 GHz downsampled pulse train (highest, blue). Dots show measured data and curves show fits to the data. The fit for the shot-noise-limited laser has a single free parameter, which is a scaling factor of order 1 due to frequency dependence of the photodetector's transimpedance gain. The fits for the pulse trains have a scaling factor in common, and have as an additional parameter the amplitude of the technical noise on the pulse train. This is -153.9 dBc/Hz for the 10 GHz pulse train and increases by a factor of $\sim$1.72 to -149.3 dBc/Hz for the 2.5 GHz downsampled pulse train. Inset: Optimized fits (dashed red) to the experimental data for the downsampled 2.5 GHz pulse train using only shot noise or linear technical noise scaling, demonstrating that both noise processes are important for explaining the data.

1.5 Model for the effect of incomplete extinction of rejected pulses and amplification of a downsampled pulse train

To this point, we have considered effects of downsampling assuming that extinction of the rejected pulses is complete, but in a practical application this is not necessarily the case. The modulators used for pulse extinction may transmit a substantial amount of energy from the rejected pulses—for example, one commercial manufacturer specifies 25 dB extinction ratio, and this number vary in practice. Additionally, the electronic gating signal may not have sufficient bandwidth to completely switch from transmission to extinction within the repetition period of the incoming pulse train, and initial extinction can be followed by some transmission caused by ringing in the gating signal. Bandwidth limitations will be increasingly likely as the repetition rates of frequency combs increase, placing more demanding requirements on gating electronics. Incomplete extinction

will add modulations to the optical spectrum and will raise the total power of the downsampled pulse train while keeping the energy of the fully-transmitted pulses fixed. This will require higher average power to achieve a given target pulse energy.

The effects of incomplete extinction of rejected pulses are exacerbated if the incomplete extinction does not happen in a deterministic and repetitive fashion; this could occur, for example, if intermediate pulses fall near the edge of the gate in the presence of relative timing jitter between the optical and electronic pulse trains, or if the extinction ratio fluctuates in time. Interestingly, if the downsampled pulse train is subsequently amplified and spectrally broadened, the impact of incomplete extinction depends on whether the optical amplifier used operates in the linear regime or in the saturated regime.

As an example, we consider the case where each fully transmitted pulse is preceded and followed by partially-extinguished pulses whose amplitudes fluctuate for each period of the downsampled pulse train. This fluctuation could occur because the pulses lie on the edge of the electronic gate and there is relative timing jitter between the optical pulse train and the gating signal. It is true that these fluctuations will lead to decoherence during nonlinear spectral broadening. However, the coherence is degraded by this mechanism only within the bandwidth that is achieved by the broadened, partially-extinguished pulses. In efficient $f - 2f$ interferometry only the fully-transmitted pulses should reach an octave in bandwidth. Therefore, this mechanism of supercontinuum decoherence is not a problem in $f - 2f$ interferometry in general, unless there is coupling between the amplitudes of the amplified partially-extinguished pulses and the amplified fully-transmitted pulses. This coupling can arise, for example, through amplification in the saturation regime, which then leads to decoherence across the full bandwidth of the supercontinuum.

To illustrate this point, we have performed numerical simulations of the spectral broadening of a 100 GHz train of 100 fs pulses which has been downsampled to 10 GHz and then amplified. We use an adaptive [9] split-step Fourier method [10] to simulate spectral broadening in 30 cm of HNLF according to the generalized nonlinear Schrodinger equation [11] (see Appendix **??**). In the simulation each fully-transmitted pulse, amplified to 1 nJ, is preceded and followed by partially-

extinguished pulses with normally distributed and uncorrelated energies with mean of 0.3 nJ and standard deviation of 0.225 nJ. This models the effect of adjacent pulses that coincide with the edge of the gate. We simulate amplification in two regimes: saturation is simulated using a fixed-energy method wherein the pulse energies in each three-pulse burst are rescaled by a common factor so that the total energy is 1.6 nJ; linear amplification is simulated using a fixed-gain model, which involves no such rescaling of pulses. Numerically, we simulate the spectral broadening of each pulse individually, which is acceptable because terms in the generalized nonlinear Schrodinger equation operate only locally or, in the case of the Raman term, on the timescale of several femtoseconds, while the separation between the pulses in each burst is 10 ps (the inverse of the initial 100 GHz repetition rate). We have verified that during simulated time-evolution each broadened pulse remains well-centered in its 5 ps simulation window.

Results of this study are shown in Figure 1.5. Figure 1.5a depicts a three-pulse burst before and after propagation in HNLF. In Figure 1.5b we show spectra corresponding to spectral broadening of this three-pulse burst, as well as plots of the spectral coherence averaged over many simulations. The first-order spectral coherence $g_{12}^{(1)}(\lambda)$ is defined as:

$$\left| g_{12}^{(1)}(\lambda) \right| = \left| \frac{\langle E_1^*(\lambda) E_2(\lambda) \rangle}{\sqrt{\langle |E_1(\lambda)|^2 \rangle \langle |E_2(\lambda)|^2 \rangle}} \right| = \left| \frac{\langle E_1^*(\lambda) E_2(\lambda) \rangle}{\langle |E(\lambda)|^2 \rangle} \right|. \tag{1.5}$$

Curves are plotted for the fixed-gain and fixed-energy cases, as well as for the case with ideal downsampling (no partially-extinguished pulses) and only shot-noise on the pulse train. The averages in the formula above are over 1000 instantiations of the pair E_1 and E_2, for a total of 2000 broadened spectra for each pulse within the burst of three. In both the fixed-gain and fixed-energy cases the coherence is poor in the center of the spectrum, but in the fixed-gain case, which models amplification in the linear regime, the coherence is preserved in the high- and low-frequency ends of the spectrum where it is needed for self-referencing.
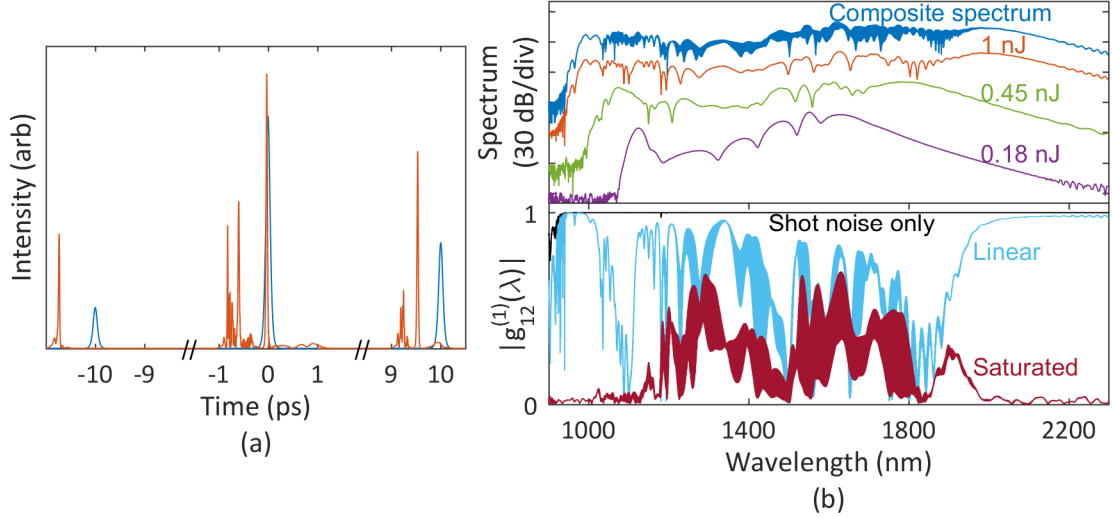
Figure 1.5: **Investigation of incomplete pulse extinction and amplification.** Investigation of incomplete pulse extinction and amplification. (a) A burst consisting of a fully-transmitted 1 nJ, 100 fs pulse and 100 fs partially-transmitted adjacent pulses with energies of 0.18 nJ and 0.45 nJ. Blue indicates initial sech^2 pulses, and orange indicates the intensity after propagation through 30 cm HNLF. Note that the x-axis has been broken. (b) Top panel: optical spectra corresponding to the pulses shown in orange in (a), showing the composite spectrum of the three pulses (top, blue) and the spectra of the 1 nJ central pulse (second, orange), the 0.45 nJ adjacent pulse (third, green), and the 0.18 nJ adjacent pulse (bottom, purple). Bottom panel: Calculated spectral coherence averaged over 2000 simulations for the case of shot-noise only (top, black) and for the case of fluctuating amplitudes of the first and last pulses as described in the text, after simulated amplification in a linear-regime optical amplifier (second, teal), and a saturated optical amplifier (bottom, maroon). For the case of linear-regime operation, high spectral coherence is preserved in the extreme ends of the supercontinuum even as it is lost in the center, in contrast with the complete loss of coherence after amplification in saturation.

1.6   Further remarks on the application of downsampling

Downsampling via pulse gating is a promising tool to manipulate high-repetition-rate frequency combs from low size, weight, and power packages and to aid in the detection of their offset frequencies. In our experiments downsampling enabled detection of f_0 at a signal-to-noise ratio sufficient for measurement and stabilization, which otherwise would have required significantly higher average power. The effects of the electronic timing jitter of the gate signal are negligible so long as incoming optical pulses do not arrive coincidentally with the edge of the gate; when they do, timing jitter induces amplitude noise on the transmitted pulses. This results in an increase in RMS optical pulse energy fluctuations σ_{PEF}. Independently, the PSD of pulse energy fluctuations may be increased

by aliasing of technical noise and by shot noise, depending on the relative magnitudes of these two types of noise. Each of these sources of signal-to-noise-ratio degradation has the potential to interfere with detection of f_0. This investigation of these challenges will facilitate application of the technique in high-repetition-rate frequency comb systems. Importantly, our experiments demonstrated that downsampling does not add a significant amount of noise to the frequency components of the pulse train, and in a separate experiment the technique has recently been used successfully to detect the carrier-envelope offset frequency of a 10 GHz comb by downsampling by a factor of four ([12], see Chapter **??**).

To employ downsampling as demonstrated here with repetition rates >10 GHz will require electronic gates with duration ≤100 ps. Technology to downsample with gates as short as 20 ps is commercially available, while 100 Gb/s integrated circuits and 25 GHz demultiplexing have been demonstrated [13, 14]. Barring the use of such state-of-the-art electronics, pulse gates of duration longer than the incoming optical pulse train's repetition period can be employed. This will be technically easier to achieve, but will result in additional modulations on the spectrum of the downsampled pulse train.

The ambiguity of the input comb's offset frequency as a result of the reduction of the offset frequency modulo the new repetition rate makes downsampling most suitable for applications where the ambiguity can be removed by some other method. Two such applications are frequency comb calibration of astronomical spectrographs, where measurement of the wavelength of a comb mode can remove the ambiguity, and microresonator-based frequency combs, where the uncertainty in the offset frequency is determined by the frequency stability of the pump laser and can be much less than the repetition rate of the downsampled comb.

References

[1] S. Backus, C. G. Durfee, M. M. Murnane, and H. C. Kapteyn. High power ultrafast lasers. *Review of Scientific Instruments*, 69 (3), **1998**, 1207. DOI: 10.1063/1.1148795 (cited on page 1).

[2] A. Baltuska, M. Uiberacker, E. Goulielmakis, R. Kienberger, V. S. Yakovlev, T. Udem, T. W. Hänsch, and F. Krausz. Phase-Controlled Amplification of Few-Cycle Laser Pulses. *IEEE Journal of Selected Topics in Quantum Electronics*, 9 (4), **2003**, 972–989 (cited on page 1).

[3] C. Gohle, J. Rauschenberger, T. Fuji, T. Udem, A. Apolonski, F. Krausz, and T. W. Hänsch. Carrier envelope phase noise in stabilized amplifier systems. 30 (18), **2005**, 2487–2489 (cited on pages 2, 9).

[4] J. Rauschenberger, T. Fuji, M. Hentschel, A.-J. Verhoef, T. Udem, C. Gohle, T. W. Hänsch, and F. Krausz. Carrier-envelope phase-stabilized amplifier system. *Laser Physics Letters*, 3 (1), **2006**, 37–42. DOI: 10.1002/lapl.200510053 (cited on page 2).

[5] M. Hirano, T. Nakanishi, T. Okuno, and M. Onishi. Silica-Based Highly Nonlinear Fibers and Their Application. *Sel. Top. Quantum Electron.*, 15 (1), **2009**, 103–113. DOI: 10.1109/JSTQE.2008.2010241 (cited on page 3).

[6] D. Mandridis, I. Ozdur, F. Quinlan, M. Akbulut, J. J. Plant, P. W. Juodawlkis, and P. J. Delfyett. Low-noise, low repetition rate, semiconductor-based mode-locked laser source suitable for high bandwidth photonic analog digital conversion. *Applied Optics*, 49 (15), **2010**, 2850–2857 (cited on page 6).

[7] J. M. Dudley, G. G. Genty, and S. Coen. Supercontinuum generation in photonic crystal fiber. *Reviews of Modern Physics*, 78 (4), **2006**, 1135–1184. DOI: 10.1103/RevModPhys.78.1135 (cited on page 6).

[8] D. C. Cole, K. M. Beha, S. A. Diddams, and S. B. Papp. Octave-spanning supercontinuum generation via microwave frequency multiplication. *Proceedings of the 8th Sympsion on Frequency Standards and Metrology 2015, Journal of Physics: Conference Series*, 723, **2016**, 012035. DOI: 10.1088/1742-6596/723/1/012035 (cited on page 10).

[9] A. M. Heidt. Efficient Adaptive Step Size Method for the Simulation of Supercontinuum Generation in Optical Fibers. *Journal of Lightwave Technology*, 27 (18), **2009**, 3984–3991 (cited on page 12).

[10] J. Hult. A Fourth-Order Runge-Kutta in the Interaction Picture Method for Simulating Su-
      percontinuum Generation in Optical Fibers. *Journal of Lightwave Technology*, 25 (12), **2007**,
      3770–3775. DOI: `10.1109/JLT.2007.909373` (cited on page 12).

[11] G. P. Agrawal. **Nonlinear Fiber Optics**. 4th. Burlington, MA: Elsevier, 2007 (cited on
      page 12).

[12] K. Beha, D. C. Cole, P. Del'Haye, A. Coillet, S. A. Diddams, and S. B. Papp. Electronic
      synthesis of light. *Optica*, 4 (4), **2017**, 406–411. DOI: `10.1364/OPTICA.4.000406` (cited on
      page 15).

[13] R. Driad, J. Rosenzweig, R. E. Makon, R. Lösch, V. Hurm, H. Walcher, and M. Schlechtweg.
      InP DHBT-Based IC Technology for 100-Gb / s Ethernet. *IEEE Trans. on Electron. Devices*,
      58 (8), **2011**, 2604–2609 (cited on page 15).

[14] D. Ferenci, M. Grozing, M. Berroth, R. Makon, R. Driad, and J. Rosenzweig. A 25 GHz Analog
      Demultiplexer with a Novel Track and Hold Circuit for a 50 GS / s A / D-Conversion System
      in InP DHBT Technology. In: **Microwave Symposium Digest**. 2012, pp. 1–3 (cited on
      page 15).